RESEARCH ARTICLE

Altered brain white matter structural motor network in spinocerebellar ataxia type 3

Xin-Yuan Chen[1,†] (iD), Zi-Qiang Huang[2,†], Wei Lin[3,†], Meng-Cheng Li[2], Zhi-Xian Ye[3], Yu-Sen Qiu[3], Xiao-Yue Xia[2], Na-Ping Chen[2], Jian-Ping Hu[2], Shi-Rui Gan[3] (iD) & Qun-Lin Chen[2] (iD)

[1]Department of Rehabilitation Medicine, The First Affiliated Hospital of Fujian Medical University, Fuzhou, China
[2]Department of Radiology, The First Affiliated Hospital of Fujian Medical University, Fuzhou, China
[3]Department of Neurology, The First Affiliated Hospital of Fujian Medical University, Fuzhou, China

Correspondence

Jian-Ping Hu and Qun-Lin Chen, Department of Radiology, The First Affiliated Hospital of Fujian Medical University, Fuzhou, China. Tel +86-13906917136 (J-PJ); +86-13509399876 (Q-LC); E-mail: fmrihjp@163.com and fychenqunlin@126.com and Shi-Rui Gan, Department of Neurology, The First Affiliated Hospital of Fujian Medical University, Fuzhou, China. Tel +86-13850172725 (S-RG); Fax +86-059187981028 (All corresponding authors); E-mail: ganshirui@fjmu.edu.cn

[†]These authors contributed equally to this study, and they are expected to be co-first authors.

Abstract

Objectives: Spinocerebellar ataxia type 3 is a disorder within the brain network. However, the relationship between the brain network and disease severity is still unclear. This study aims to investigate changes in the white matter (WM) structural motor network, both in preclinical and ataxic stages, and its relationship with disease severity. **Methods**: For this study, 20 ataxic, 20 preclinical SCA3 patients, and 20 healthy controls were recruited and received MRI scans. Disease severity was quantified using the SARA and ICARS scores. The WM motor structural network was created using probabilistic fiber tracking and was analyzed using graph theory and network-based statistics at global, nodal, and edge levels. In addition, the correlations between network topological measures and disease duration or clinical scores were analyzed. **Results**: Preclinical patients showed increasing assortativity of the motor network, altered subnetwork including 12 edges of 11 nodes, and 5 brain regions presenting reduced nodal strength. In ataxic patients assortativity of the motor network also increased, but global efficiency, global strength, and transitivity decreased. Ataxic patients showed a wider altered subnetwork and a higher number of reduced nodal strengths. A negative correlation between the transitivity of the motor network and SARA and ICARS scores was observed in ataxic patients. **Interpretation**: Changes to the WM motor network in SCA3 start before ataxia onset, and WM motor network involvement increases with disease progression. Global network topological measures of the WM motor network appear to be a promising image biomarker for disease severity. This study provides new insights into the pathophysiology of disease in SCA3/MJD.

Introduction

Spinocerebellar ataxia type 3, also known as Machado–Joseph disease (SCA3/MJD), is the most common type of autosomal dominantly inherited cerebellar ataxia in the world[1] and is caused by the cytosine–adenine–guanine (CAG) repeat expansion in the ATXN3 gene that encodes a polyglutamine (poly Q) stretch located in the carboxyl terminus of the ATXN3 protein.[2] Although there are no therapies to alter its progressive fatal course, a recent animal study demonstrates antisense oligonucleotide (ASO) targeting the SCA3/MJD disease gene is a disease-modifying therapeutic strategy for SCA3/MJD.[3]

Neuromodulation represents another promising future therapeutic approach in neurodegenerative ataxia.[4–7] What's more, interventions in the early stages of the disease are more effective than when they are used in later stages.[7–9] So, objective and effective biomarkers for disease progression from the preclinical to the ataxic stage are urgently needed for the evaluation of the clinical trials and treatment for SCA3/MJD.

The preclinical phase of spinocerebellar ataxias (SCAs) is when a person carries a gene mutation but does not yet present with cerebellar ataxia, which was recently defined by a SARA (Scale for the Assessment and Rating of Ataxia) score of <3.[10] In recent years, an increasing

number of neuroimage studies have focused on patients before an ataxic phenotype was obvious. Tissue loss of the cervical spinal cord, brainstem, pallidum, and cerebellar anterior lobe was found in preataxic SCA3/MJD mutation carriers.[11] White matter microstructural abnormalities were also present in the cerebellar and cerebral peduncles of preataxic patients.[12,13] A 7.0 T MRS study showed that neurochemical abnormalities are detectable in preclinical SCA3/MJD individuals before they manifested ataxic symptoms.[14] Nevertheless, these approaches are limited in their ability to understand the interactions between various brain regions of interest. Graph theory analysis made it possible to describe the topological organizational properties of the structural and functional brain network.[15] A recent study[16] using graph theory found that SCA3/MJD patients present with abnormalities to their structural covariance network based on three-dimensional fractal dimension values, indicating that SCA3/MJD is a complex network disorder. However, the structural covariance network cannot truly reflect the white matter fiber bundle connections across brain regions. Therefore, the study of the white matter structural network in SCA3/MJD can help to further characterize the changes in the brain structural network caused by disease at the individual level. In addition, a link between changes in the motor network of the white matter structure of the brain and motor function impairment in patients was found in diseases such as cerebellar-type multisystem atrophy[17] and multiple sclerosis.[18] However, whether the motor network of the white matter structure of the brain in SCA3/MJD patients has abnormal changes before the onset of ataxia symptoms, and the relationship between the motor network changes and the severity and course of the disease, is still unclear.

To fill the current research gap, we used probabilistic tractography in this study, which is capable of resolving the problem of crossing fibers in white matter voxels,[19] to characterize the brain organization of the motor network in SCA3/MJD. Motor networks have been studied in other neurodegenerative diseases comprising the precentral cortex, basal ganglia, thalamus, ventral diencephalon, and cerebellum.[17,20–23] We used network-based statistics (NBS),[24] a statistical approach that identifies connections in a graph that may be relevant to diagnostic status,[25] to find different subnetworks in preclinical and ataxic SCA3/MJD patients. Given that previous imaging studies have shown that morphological changes already occur in the cerebellum at the preataxic stage, we hypothesized that motor network abnormalities are already detectable before the onset of ataxia, and motor network alterations are associated with disease severity in SCA3/MJD.

Methods

Subjects and clinical assessments

We recruited 20 preclinical and 20 ataxic SCA3/MJD patients from the outpatient Department of Neurology at the First Affiliated Hospital of Fujian Medical University. Twenty age and sex-matched healthy controls (HCs) were included. All patients underwent genetic testing to identify CAG repeats. Genetic counseling was offered for all asymptomatic participants before diagnostic genetic testing, and genetic status was informed upon the participant's request. As a routine examination, the results of conventional MRI (T1-WI, T2-WI, and DWI) were reported to the participant. All participants, before enrollment, underwent a detailed manifest evaluation to exclude any patients with a family history of neurological/psychiatric diseases, systemic metabolic diseases, or tumors. All participants were right-handed. The International Cooperative Ataxia Rating Scale (ICARS) and Scale for the Assessment and Rating of Ataxia (SARA) were used to assess disease severity. Using a SARA cutoff value of 3, SCA3/MJD mutation carriers were divided into preclinical (SARA <3) and ataxic (SARA ≥3) individuals.[10] All subjects gave their written informed consent before study participation. All procedures performed involving human participants were approved by the Ethics Committee of the First Affiliated Hospital of Fujian Medical University in China.

MRI scanning

MRI acquisition was performed on a 3 T Siemens Skyla scanner at the Imaging Center of the First Affiliated Hospital of Fujian Medical University. For all MR procedures, the head was immobilized using self-expanding foam cushions.

Volumetric (3D) T1-weighted images were acquired with the following imaging parameters: repetition time (TR) = 2300 ms, echo time (TE) = 2.3 ms, inversion time (TI) = 900 ms, flip angle = 8°, field of view (FOV) = 240 mm × 256 mm, matrix size = 240 × 256, bandwidth = 200 Hz/Px, slices = 192, voxel size = 1 mm × 1 mm × 1 mm and total acquisition time = 5 min 12 s.

DWI was acquired with the following imaging parameters: TR = 11,700 ms, TE = 96 ms, the field of view = 232 mm × 232 mm, matrix size = 116 × 116, voxel size = 2 mm × 2 mm × 2 mm, slice spacing = 0, slice number = 80, NEX = 1, total acquisition time = 12 min 54 s. DWI was acquired at b-values of 1000 and 2000 s/mm^2 along 30 uniformly distributed directions with a spin-echo echo-planar imaging scheme

in an anterior–posterior phase encoding direction. The same diffusion directions were used for each shell. Each DWI acquisition was complemented with a non-weighted diffusion image ($b = 0$ s/mm^2).

Gradient echo sequences are used to acquire a field map with the following parameters: repetition time (TR) = 580 ms, echo time (TE) = 7.38 ms, flip angle = 60°, slice number = 54, slice thickness 3 mm, Slice Space 0.75 mm, field of view (FOV) = 232 × 232, matrix size = 78 × 78, voxel size = 2.94358 mm × 2.94358 mm × 3 mm and total acquisition time = 1 min 33 s.

MRI data processing

T1WI

The T1-weighted images were firstly registered to a diffusion space using boundary-based registration (BBR) in the Functional MRI of the Brain (FMRIB) Software Library, Version 6.0.[26] To delineate the nodes accurately, the cerebral and cerebellar cortex were parcellated separately using two atlantes: the Desikan-Killiany (DK) atlas[27] from FreeSurfer v6.0[28] and a probabilistic anatomic atlas from SUIT toolbox.[29,30]

DWI

The first preprocessing step was denoising and removing Gibbs' ringing artifacts in the DWI image using the MRtrix3 package.[31] Then, *fsl_prepare_fieldmap* was used to acquire a field map which was then aligned to the corresponding b0 map with rigid body registration in the FMRIB Software Library. Next, *fugue* (FMRIB's Utility for Geometrically Unwarping EPIs) was used to correct geometric distortion. The GPU version of the eddy was used to correct eddy currents, inter-and intra-volume subject movements, and signal dropout.[32–34] DWI was performed with a B1 field in homogeneity correction using the N4 algorithm as described in ANTs.[35]

Response function and fODF estimation for probabilistic MSMT-CSD tracking

The whiter matter (WM), gray matter (GM), and cerebrospinal fluid (CSF) response functions were estimated without a T1 image for Multi-shell, Multi-tissue (MSMT), and Constrained Spherical Deconvolution (CSD).[36] Next, the WM fiber orientation distribution function (fODF), GM fODF, and CSF fODF were obtained using the *dwi2-fod* command with the *msmt-csd* option, and data were then normalized using the *mtnormalise* command. The normalized WM fODF here was used for probabilistic MSMT-CSD tracking.

Fiber tracking

For probabilistic MSMT-CSD tracking, second-order integration was employed over the FOD (iFOD2) algorithm[37] using the following parameters: step size, 1.0 mm; maximum curvature, 45° per step; length, 4–250 mm; fiber orientation distribution threshold, 0.05 for probabilistic MSMT-CSD tracking. In total, 10^7 streamlines were seeded from WM fODFs. Anatomically constrained tractography (ACT)[38] frameworks were applied to confine the streamlines to the volume of the brain white matter by making effective use of the information available from anatomical image segmentation. Furthermore, 'backtracking' and 'crop_at_gmwmi' were used within the ACT framework to allow tracks to be truncated and re-tracked if a poor structural termination was encountered and crop streamline endpoints more precisely as they cross the gray matter-whiter matter interface. The interface mask was obtained using the *5tt2gmwmi* command and was treated as a seeding point for fiber tracking. We then applied the spherical deconvolution-informed filtering of tractograms (SIFT2) algorithm[39] to reduce biases by determining an appropriate cross-sectional area multiplier for each streamline.

Construct matrix

WM connectivity was modeled as a weighted, undirected network. Nodes were represented by 118 distinct regions, and for each possible node pair, interregional connectivity was defined as the number of streamlines multiplied by the fractional anisotropy (FA), representing the edges of the connectome. Pairs of larger brain regions have higher streamline counts by virtue of being larger targets. To account for the variation in brain region size, we divided each edge by the average volume of the pairs of brain regions.[40] The diagonal elements represented self-connections and were set as zeros. This resulted in a 118 × 118 symmetric interregional connectivity matrix. Finally, based on our hypothesis of differences in the motor network, we extracted 46 regions of interest (ROIs) to create a 46 × 46 motor network. The ROIs selected to include the bilateral precentral cortex, basal ganglia, thalamus, ventral diencephalon, and 24 cerebellar areas.

Graph theory analyses

Only the above-described motor network was analyzed at various levels of granularity: the edge level, the node level (local), and the entire network level (global). The brain connectivity toolbox[15] was used for computing the topological features of the graph. The following five global network measures were computed: assortativity,

characteristic path length, global efficiency, global strength, and transitivity. In addition, one local network measure was computed: nodal strength. Functional segregation in the brain is the ability for specialized processing to occur within densely interconnected groups of brain regions.[15] The transitivity is the ratio of triangles to triplets in a network and quantifies the proportion of fully connected triads of regions whose neighbors are also immediate neighbors of each other, with high transitivity indicating increased local connectivity.[41,42] Functional integration in the brain is the ability to rapidly combine specialized information from distributed brain regions.[15] The characteristic path length is the average shortest path length in the network. The global efficiency is the average inverse shortest path length in the network. Both global efficiency and characteristic are measures of functional integration. Nodal strength is the sum of the weights of links connected to the node. Node strength can be a measure of centrality to find individual nodes which often interact with many other regions, facilitate functional integration, and play a key role in network resilience to damage. Global strength is the average of the strengths across all nodes in a network.[43]

Statistical analysis

All of the following analyses were performed using R Software for Statistical Computing, version 4.1.1. R Foundation for Statistical Computing, Vienna.

Demographic and clinical variables

The analysis of differences between groups was performed by the Kruskal-Wallis test for age, the chi-square test for sex groups, and Mann–Whitney U test for CAG repeats.

Global and nodal levels

To investigate group differences in network topology measures between ataxic SCA3/MJD patients, preclinical patients, and HCs, we applied the nonparametric permutation test (10,000 permutations) to calculate the F statistics and p-values in an one-way ANOVA design (model) and set age as a control variable, which can be fulfilled by the function **aovperm** in the R package **permuco**.[44] In all measures that showed a significant group difference after multiple testing corrections, the nonparametric permutation test was used to perform additional post hoc pairwise comparisons using the function **perm.t.test** in R package **Mkinfer**[45] through the regression analysis, age as a control variable was excluded. To identify factors between preclinical patients and ataxic patients, we applied linear regression analysis, in which CAG repeat

was excluded as well. The relationships between network measures that showed significant group differences across the duration, SARA, and ICARS scores in the ataxic group were analyzed using partial correlations, with age as a covariate. The Bonferroni correction (FWER) was applied to correct for multiple comparisons, using a significance threshold of $P < 0.05$.

Edge level

The network-based statistics (NBS) toolbox introduced by Zalesky et al.[24] was utilized for performing edge-wise analyses to identify subnetworks (clusters of nodes and edges) comprising connections with reduced connectivity strength in preclinical and ataxia SCA3/MJD patients. In brief, a two-sample *t*-test was independently performed at each edge to test the null hypothesis of equality in mean connectivity strength, with age as a nuisance variable, between patients and controls. A set of suprathreshold edges was defined by applying a primary component-forming threshold ($t = 3.5$, two-tailed *t*-test) to the test statistic computed for each edge. The statistical significance of each connected component was obtained concerning an empirical estimate of the null distribution of maximal component sizes (5000 permutations), with the component size measured as the sum of the weighted edges it comprised. We reported any components that were significant at a *p*-value of 0.05 after family-wise error correction.

Results

Demographic and clinical variables

Finally, 20 preclinical patients, 20 patients with ataxia, and 20 HCs were included. The demographic and clinical features of the three groups of subjects are shown in Table 1. There were no significant differences between patients in the HC group, the preclinical group, and the ataxia group in terms of age and sex. Compared with the number of CAG repeats in preclinical patients, the number of CAG repeats in ataxia patients was significantly higher, and the difference was statistically significant ($P < 0.0001$).

White matter structural motor network

Global level

The statistically significant global properties of the motor network, after multiple comparison corrections, across the three groups include transitivity, assortativity, global strength, and global efficiency. The results of post hoc
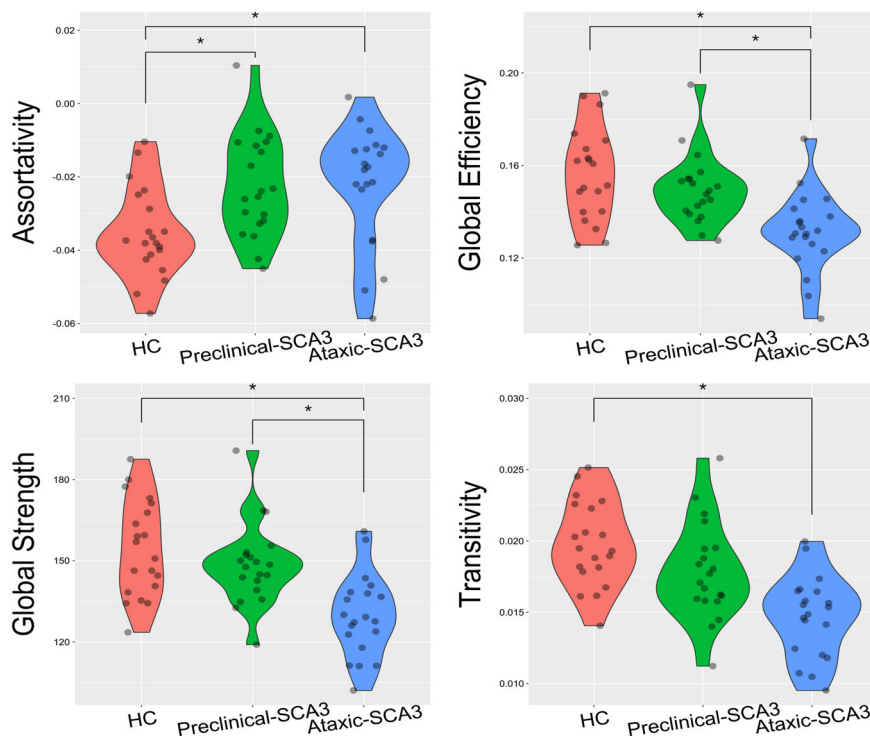
Table 1. Demographic and clinical variables.

	HC	Preclinical-SCA3/MJD	Ataxia-SCA3/MJD	P value
Sex (M/F)	8/12	8/12	10/10	0.7622
Age (years)	29.80 ± 9.20	29.95 ± 10.16	29.95 ± 4.31	0.7699
Age of onset (years)	–	–	23.52 ± 4.64	–
Disease duration (years)	5.70 ± 3.53	–	–	–
CAG repeats	–	73 ± 4.67	77.75 ± 1.77	**0.0001**
SARA score	–	–	9.15 ± 4.26	–
ICARS score	–	–	21.68 ± 11.69	–

Values are represented as the mean ± SD; Bold values indicate statistical differences; ICARS, International Cooperative Ataxia Rating Scale; SARA, Scale for the Assessment and Rating of Ataxia.

comparisons are as follows: compared with the HC group, the assortativity of the motor network in preclinical patients increased ($t = 3.131$, $P = 0.0030$), and there was no significant difference in the transitivity, global efficiency, or global strength ($t = 1.912$, $P = 0.0623$; $t = 1.223$, $P = 0.2268$; $P = 0.2554$, $t = 1.138$, respectively).

Compared with the HC group, the assortativity of motor network in patients with ataxia increased ($t = -2.906$, $P = 0.0067$), but the global efficiency, global intensity, and transitivity were significantly reduced ($t = 4.303$, $P = 0.0001$; $t = 4.781$, $P < 0.0001$; $t = 5.616$, $P < 0.0001$). The global efficiency and global strength in patients with ataxia decreased significantly compared with preclinical patients ($t = 3.604$, $P = 0.0005$; $t = 3.391$, $P = 0.0022$). The significant global level differences in the motor network of the three groups are shown in Figure 1.

Edge level

In preclinical patients relative to HCs, NBS analysis revealed reduced connectivity in preclinical patients, including 12 edges connecting 11 nodes ($P = 0.0052$). In ataxic patients relative to HCs, NBS identified one subnetwork, including 38 nodes and 242 decreased connections ($P < 0.0002$). In ataxic patients relative to preclinical patients, NBS analysis revealed significantly lower connectivity in ataxic patients involving 22 edges and 16 nodes ($P = 0.0020$). The edge level differences in the motor network between the three patient groups are shown in Figure 2.

Nodal level

A total of 44 brain regions with statistically different nodal strengths after multiple comparison corrections

Figure 1. The significant global level differences of the motor network of three groups; *Represents statistically significant differences between groups; the HC group, the healthy control group.
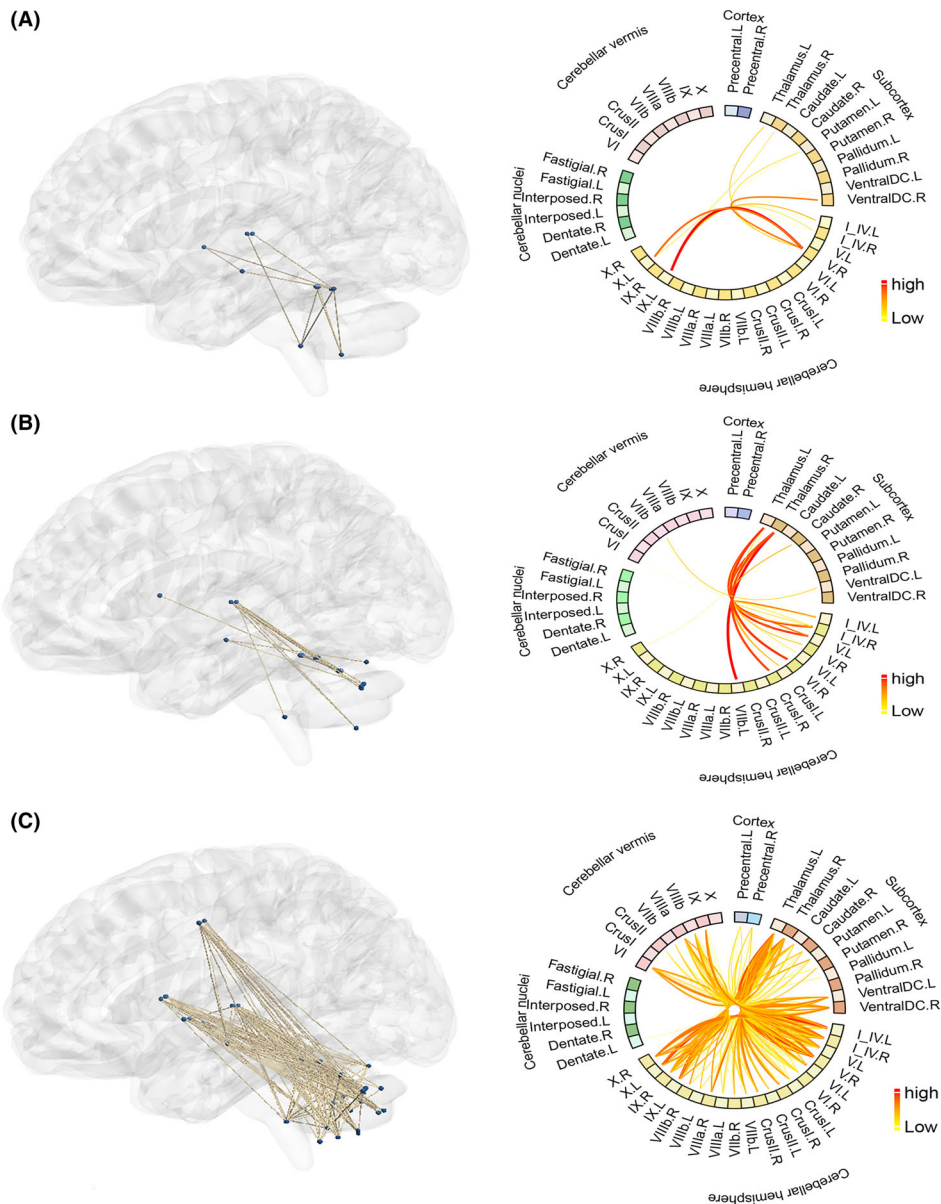
Figure 2. NBS analysis reveals reduced connectivity in the preclinical SCA3 patients compared with HC (A), ataxic SCA3 patients compared with preclinical SCA3 patients (B), and ataxic SCA3 compared with HC (C); The reduced edges in the subnetwork shown in a brain model and a circle in the circle plot, The color and thickness of the edges represent how significantly the two groups are different. The redder and coarser it is, the greater the difference.

were found among the three groups of subjects. The results of post hoc comparisons are as follows: 5 regions with significantly reduced nodal strength within the motor network were observed in preclinical patients compared to HCs, including the left putamen, right ventral diencephalon, left cerebellar lobule I_IV, and bilateral cerebellar lobules V. There were 44 regions with significantly reduced nodal strength in the motor network of ataxic patients in comparison to preclinical patients or

HCs. The nodal level differences between the three groups of subjects are shown in Table 2.

The correlation between network measures and clinical features

A significant negative correlation was observed between the transitivity of the motor network and the SARA score ($r = -0.662105486$, corrected $P = 0.0010$) and the ICARS

Table 2. Differences in motor network nodal strengths across preclinical SCA3/MJD patients, ataxia SCA3/MJD patients, and healthy controls.

Node	ANOVA			Post hoc pairwise comparison *P* value (*t*)		
	P	*F*	corrected *P* value	HC vs. Preclinical-SCA3/MJD	HC vs. Ataxic-SCA3/MJD	Preclinical-SCA3/MJD vs. Ataxic SCA3/MJD
Cortex						
Precentral.L	0	266	0.0046	0.7683 (−0.285)	**0 (21.16)**	**0 (25.611)**
Precentral.R	0	265	0.0046	0.32 (−1.023)	**0 (19.792)**	**0 (27.831)**
Subcortex						
Thalamus.L	0	683	0.0046	0.8888 (0.146)	**0 (36.387)**	**0 (37.844)**
Thalamus.R	0	548	0.0046	0.8687 (0.18)	**0 (29.528)**	**0 (41.272)**
Caudate.L	0	424	0.0046	0.9247 (0.095)	**0 (28.342)**	**0 (30.823)**
Caudate.R	0	348	0.0046	0.868 (0.169)	**0 (25.229)**	**0 (33.976)**
Putamen.L	0	398	0.0046	**0.0114 (2.666)**	**0 (28.614)**	**0 (30.871)**
Putamen.R	0	416	0.0046	0.0262 (2.325)	**0 (26.734)**	**0 (34.696)**
Pallidum.L	0	415	0.0046	0.9575 (0.053)	**0 (32.864)**	**0 (29.063)**
Pallidum.R	0	440	0.0046	0.7965 (0.262)	**0 (33.528)**	**0 (27.876)**
VentralDC.L	0	428	0.0046	0.0272 (2.335)	**0 (28.552)**	**0 (30.558)**
VentralDC.R	0	317	0.0046	**0.0085 (2.778)**	**0 (26.006)**	**0 (24.639)**
Cerebellar hemisphere						
I_IV.L	0	364	0.0046	**0.0045 (2.981)**	**0 (26.6)**	**0 (29.359)**
I_IV.R	0	271	0.0046	0.0222 (2.41)	**0 (23.061)**	**0 (24.95)**
V.L	0	297	0.0046	**0.0135 (2.567)**	**0 (24.17)**	**0 (26.791)**
V.R	0	349	0.0046	**0.0004 (3.532)**	**0 (29.034)**	**0 (24.696)**
VI.L	0	303	0.0046	0.4465 (0.766)	**0 (23.128)**	**0 (28.75)**
VI.R	0	256	0.0046	0.1775 (1.361)	**0 (22.497)**	**0 (22.847)**
CrusI.L	0	444	0.0046	0.5807 (−0.554)	**0 (25.749)**	**0 (40.994)**
CrusI.R	0	358	0.0046	0.3842 (0.868)	**0 (25.008)**	**0 (30.684)**
CrusII.L	0	381	0.0046	0.4774 (0.715)	**0 (25.578)**	**0 (30.402)**
CrusII.R	0	319	0.0046	0.46 (0.748)	**0 (23.519)**	**0 (27.489)**
VIIb.L	0	315	0.0046	0.8958 (−0.137)	**0 (26.409)**	**0 (24.007)**
VIIb.R	0	162	0.0046	0.6659 (−0.44)	**0 (18.81)**	**0 (17.268)**
VIIIa.L	0	208	0.0046	0.6802 (0.42)	**0 (29.652)**	**0 (15.99)**
VIIIa.R	0	217	0.0046	0.4633 (−0.74)	**0 (20.772)**	**0 (21.113)**
VIIIb.L	0	118	0.0046	0.9008 (−0.128)	**0 (19.941)**	**0 (12.448)**
VIIIb.R	0	148	0.0046	0.342 (−0.954)	**0 (18.094)**	**0 (16.595)**
IX.L	0	221	0.0046	0.0561 (1.978)	**0 (21.764)**	**0 (20.575)**
IX.R	0	188	0.0046	0.9694 (0.038)	**0 (21.227)**	**0 (17.866)**
X.L	0	147	0.0046	0.2309 (1.215)	**0 (26.257)**	**0 (12.575)**
X.R	0	179	0.0046	0.4226 (0.799)	**0 (24.063)**	**0 (15.473)**
Cerebellar nuclei						
Dentate.L	0	31	0.0046	0.8949 (−0.139)	**0 (8.558)**	**0 (7.358)**
Dentate.R	0	26.0	0.0046	0.2483 (−1.195)	**0 (7.405)**	**0 (6.848)**
Interposed.L	0	12	0.0046	0.5046 (−0.671)	**0 (4.356)**	**0 (5.376)**
Interposed.R	0	19.0	0.0046	0.1773 (−1.396)	**0 (5.103)**	**0 (8.72)**
Fastigial.L	0	5.10	0.4002	-	-	-
Fastigial.R	0	8.84	0.0046	0.0167 (−2.245)	**0.0012 (3.077)**	**0 (3.202)**
Cerebellar vermis						
VI	0	250	0.0046	0.017 (2.458)	**0 (21.831)**	**0 (24.36)**
CrusI	0	0.778	1	-	-	-
CrusII	0	46.6	0.0046	0.3202 (−1.014)	**0 (8.376)**	**0 (11.613)**
VIIb	0	86.1	0.0046	0.4162 (−0.842)	**0 (13.169)**	**0 (13.774)**
VIIIa	0	247	0.0046	0.419 (0.804)	**0 (30.53)**	**0 (17.799)**
VIIIb	0	110	0.0046	0.7045 (−0.38)	**0 (16.193)**	**0 (13.587)**
IX	0	97.4	0.0046	0.3443 (−0.935)	**0 (13.671)**	**0 (13.827)**
X	0	21	0.0046	0.4712 (−0.75)	**0 (6.253)**	**0 (5.496)**

The comparison of the differences between the three groups and the post hoc pair test was performed using the permutation test; the Bonferroni correction was used, and the *P* < 0.05/3 was considered to be statistically different; statistically significant differences are indicated by bold lettering; the HC group, the healthy control group.
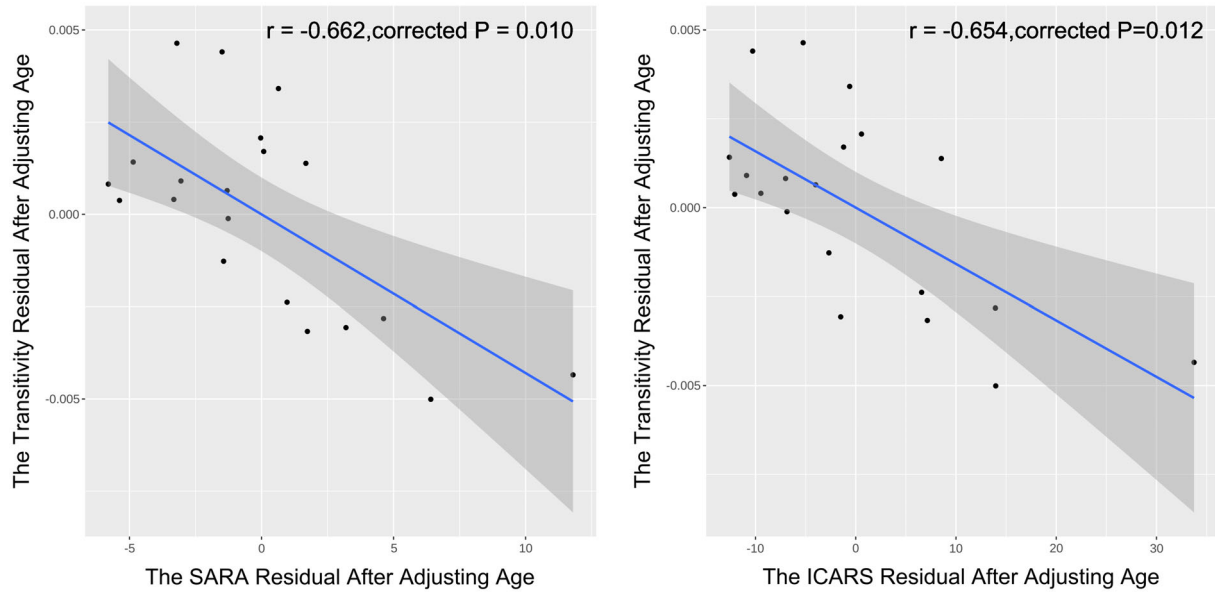
Figure 3. Correlation between transitivity of motor network and SARA score and ICARS score; SARA = Scale for the Assessment and Rating of Ataxia; ICARS, International Cooperative Ataxia Rating Scale.

score ($r = -0.654383419$, corrected $P = 0.012$) in ataxic patients (Fig. 3) after controlling for age. In addition, after controlling for covariates of age and CAG repetitions, negative correlations could still be observed between the transitivity of the motor network and the SARA score ($r = -0.613$, $P = 0.0340$ after correction) and the ICARS score ($r = -0.607$, $P = 0.0375$ after correction). No significant correlation was found between the other global or nodal measures and disease severity or duration.

Discussion

To the best of our knowledge, this is the first study focused on white matter network abnormalities in SCA3/MJD, including both preclinical and ataxia stages, and this study offers a unique opportunity to explore the pathophysiological mechanisms that manifest in the initial stages of SCA3/MJD. In this cross-sectional MRI study, we showed that structural brain network abnormalities in preclinical patients precede the onset of ataxia symptoms at global, nodal, and edge levels. A significant correlation between the transitivity of the motor subnetwork and disease severity was observed. There was a greater node and edge involvement in preclinical patients relative to ataxic patients.

Of note, global efficiency and characteristic path length of the motor network are not affected in preclinical patients, which are measures of functional integration that reflect the ability to rapidly combine specialized

information from distributed brain regions.[15] Conversely, transitivity is already altered in the preclinical stage and is a measure of functional segregation that reflects the ability of specialized processes to occur within highly interconnected groups of brain regions.[15] Therefore, our results suggest an impairment of the efficiency of local information transfer, processing, and preservation of global integration, likely reflecting a reduced competence in information exchange between adjacent brain areas in the motor network in the disease's early stage. As SCA3/MJD progressed, a global efficiency decrease was observed in the ataxic stage, reflecting that the ability to exchange information between distant brain areas is impaired. A previous SCA3/MJD image study focused on the whole brain network using the gray matter three-dimensional fractal dimension (3D-FD) values and reported that the global efficiency decreased and character path length increased, resulting in a loss of small-world topology, which is similar to the findings of our study. While the relationship between the whole-brain network and the motor network is not very clear, it is presumed that a change in the motor network accounts for a part of the abnormality observed in the whole-brain network.

As a measure of network resilience,[15] assortativity reflects a network's vulnerability to insult. When network hubs are abnormally clustered and connected to other high-degree nodes, assortativity increases but the network becomes less efficiently wired.[46] A recent whiter matter network diffusion-weighted image study similarly showed that children with perinatal stroke present with a higher

global assortativity in the intact contralesional hemisphere, and this was associated with better motor performance and lower assortativity values.[47] In this study, assortativity values were increased in both preclinical and ataxic patients compared to HCs. This result suggests that brain regions in the motor network are changed to preferentially connect with other brain regions with similar strength as SCA3/MJD progresses. These findings may reflect the neurodegenerative mechanisms that lead to the segregation of the motor network into two sub-network, composed of either high- or low-strength nodes. We propose that this abnormality may lead to an increase in wiring costs and a decrease in efficiency.

NBS analysis reveals structural connectivity decreases between the left putamen, right diencephalon, bilateral thalamus, and some cerebellum lobules, mostly located in the anterior cerebellar lobe in the preclinical group. This result reflects cerebral-cerebellar connectivity disruption, which is also found in other types of ataxia.[24,48,49] A recent neuroimage study[12,50] in preclinical SCA3/MJD patients reported white matter fiber damage in the bilateral cerebellar peduncles and cerebellum. As a bridge between the cerebellum and other brain areas, the WM fiber damage in cerebellum peduncles decreases the structural connectivity between the cerebellum, thalamus, and base ganglia, which may lead to a change in the motor network of patients with preclinical SCA3/MJD. A recent structural MRI study[11] reported that preataxic mutation carriers show tissue loss in the spinal cord, pallidum, and cerebellar anterior lobe compared to controls, and this was also found in our study.

Nodes of high strength serve central roles in network organization and are thought to be critical for information exchange. A region with reduced nodal strength indicates disruption of interconnectivity with other regions in the network and decreasing in the network information transmission process. In this study, reduced nodal strength was observed in the left cerebellar IV, bilateral cerebellar V, right ventral diencephalon, and left putamen in the preclinical stages of the disease. Previously, a nuclear medicine image study found that 5 asymptomatic SCA3/MJD carriers presented with decreased dopamine-related neuronal function in the striatal region, especially in the putamen.[51] Similarly, we also found an abnormality in the left putamen that decreased nodal strength in the asymptomatic stage. Damage to the anterior lobe of the cerebellum may result in ipsilesional spontaneous nystagmus which can be an early symptom for some patients with isolated cerebellar infarction in the territory of the superior cerebellar artery.[52] The cerebellar anterior lobe is predominantly involved in the early stages of disease in this study. This information might be considered to pave the way for the study in terms of nystagmus which is

reported to be one of the early symptoms before ataxia in the course of SCA3/MJD.[10,53] The above results indicate that in the early disease process, both intracerebellar and extracerebellar brain areas appear to undergo topological changes, which may lead to a decline in information transmission across the motor network.

Both edge-level and nodal-level results show that a larger scope of abnormalities in brain regions and structural connections was detected in ataxia patients compared to preclinical patients or HCs. The extent of damage to the motor network gradually increased alongside disease progression. Of note, the transitivity, as a quantitative indicator, was associated with increased CAG and ICARS scores in the ataxic group. All of the above are in line with the gradual worsening of patients' clinical symptoms. In line with our results, the putamen, thalamus, and cerebellum shrank significantly after 5 years in SCA3.[54] The cerebellum and basal ganglia are densely interconnected in humans.[55] Thus, atrophy at one node can spread throughout the entire network to influence other nodes.[55,56] As shown by SCA3 patients in our study, the two subcortex systems involving the ganglia and cerebellum tend to be isolated from each other. It is important to note that compared with preataxic patients, abnormal structural connections in ataxic patients are mainly linked with the bilateral thalamus. Ataxia patients experiencing essential tremors can have symptoms improved, deteriorated, or induced by thalamic stimulation.[57–59] It is speculated that the thalamus plays a core role in the emergence of ataxia in SCA3/MJD disease.

A network is a mathematical representation of a real-world complex system and is defined by a collection of nodes and links between pairs of nodes. In this study, the node is the brain region and the link is whiter matter fibers. So, the definition of node and link largely determine the neurobiological interpretation of network topology. In order to delineate cerebellum parcellation accurately, we used a spatially unbiased atlas template.[29] The most common approach to tractography is to use the diffusion tensor model to estimate the orientation of the white matter fibers, coupled with a simple, streamlined algorithm to follow these directions, and hence delineate the pathways.[19] The diffusion tensor model is only capable of resolving a single fiber's orientation per voxel, so it can be unsuitable when voxels have multiple fiber orientations. This can be a serious limitation, given that a majority of brain voxels contain crossing whiter fibers.[60] Probabilistic tractography algorithms that estimate multiple fiber directions have been proposed to overcome this limitation. Constrained spherical deconvolution (CSD) can improve the reliability of whole-brain tractography using a high-quality fiber orientation distribution function (fODF) but cannot yield accurate fODFs in voxels

containing GM and cerebrospinal fluid (CSF), which has an impact on reconstructing the gray matter-white matter interface. Thus, we use probabilistic MSMT-CSD tracking[36] to overcome the above problems.

Our present study is not without limitations. First, this is a cross-sectional study and the sample size is small. the age of ataxia onset in the preclinical group is unclear in our study, so precise relationships cannot be established between topological metrics and disease duration from a full disease course. A longitudinal study must recruit more subjects to verify our results. Second, the voxel size for acquiring a diffusion-weighted image is 2 mm. The accuracy of fiber orientation estimation is degraded for 2 mm voxels, particularly for areas of complex axonal configurations,[61] which effects the overall accuracy of tractography. Improving image resolution requires a longer acquisition time with no patient movement, which can be difficult for SCA3/MJD patients experiencing involuntary movements. Third, we did not evaluate the non-motor symptoms of SCA3/MJD, such as cognitive and psychiatric symptoms, which may alter the brain network as cofounding factors. Fourth, we used the SUIT toolbox to segment and parcellate the cerebellum especially, but this is not a state-of-the-art cerebellum parcellation. Machine learning-based methods provide a more efficient and accurate parcellation.[62]

Conclusions

Changes to the white matter motor network in spinocerebellar ataxia type 3 start before ataxia onset and the involvement of the white matter motor network increases alongside disease progression. Global network topological measures of the white matter motor network appear to be a promising image biomarker reflecting the progression of spinocerebellar ataxia type 3. This study provides new insights into the pathophysiology of disease in SCA3/MJD. Future studies could investigate the relationship between structural and functional motor network changes to better understand the pathophysiological mechanisms involved in disease progression.

Author Contributions

The work reported above for publication was completed by all authors: Xin-Yuan Chen, Zi-Qiang Huang, and Wei Lin for study design, paper writing, and data processing; and Meng-Cheng Li, Xiao-Yue Xia, and Na-Ping Chen contributed to magnetic resonance scanning and processing. Zhi-Xian Ye and Yu-Sen Qiu collected the data from patients. Jian-Ping Hu, Shi-Rui Gan, and Qun-Lin Chen helped in manuscript preparation and contributed to the supervision of the whole process. All authors contributed to the article and approved the submitted version.

Conflict of Interest

The authors declare that they have no conflict of interest.

Informed Consent

Informed consent was obtained from all individual participants included in the study.

Data Availability Statement

The data sets used or analyzed during the current study are available from the corresponding author on reasonable request.

References

1. Ruano L, Melo C, Silva MC, Coutinho P. The global epidemiology of hereditary ataxia and spastic paraplegia: a systematic review of prevalence studies. Neuroepidemiology. 2014;42(3):174-183.

2. Toulis V, Garcia-Monclus S, de la Pena-Ramirez C, et al. The deubiquitinating enzyme ataxin-3 regulates ciliogenesis and phagocytosis in the retina. Cell Rep. 2020 Nov 10;33(6):108360.

3. McLoughlin HS, Moore LR, Chopra R, et al. Oligonucleotide therapy mitigates disease in spinocerebellar ataxia type 3 mice. Ann Neurol. 2018 Jul;84(1):64-77.

4. Benussi A, Cantoni V, Manes M, et al. Motor and cognitive outcomes of cerebello-spinal stimulation in neurodegenerative ataxia. Brain. 2021;144(8):2310-2321.

5. Benussi A, Dell'Era V, Cantoni V, et al. Cerebello-spinal tDCS in ataxia: a randomized, double-blind, sham-controlled, crossover trial. Neurology. 2018;91(12):e1090-e1101.

6. Benussi A, Dell'Era V, Cotelli MS, et al. Long term clinical and neurophysiological effects of cerebellar transcranial direct current stimulation in patients with neurodegenerative ataxia. Brain Stimul. 2017;10(2):242-250.

7. Miterko LN, Lin T, Zhou J, et al. Neuromodulation of the cerebellum rescues movement in a mouse model of ataxia. Nat Commun. 2021;12(1):1295.

8. Ashizawa T, Oz G, Paulson HL. Spinocerebellar ataxias: prospects and challenges for therapy development. Nat Rev Neurol. 2018;14(10):590-605.

9. Zu T, Duvick LA, Kaytor MD, et al. Recovery from polyglutamine-induced neurodegeneration in conditional SCA1 transgenic mice. J Neurosci. 2004;24(40):8853-8861.

10. Maas RP, van Gaalen J, Klockgether T, van de Warrenburg BP. The preclinical stage of spinocerebellar ataxias. Neurology. 2015;85(1):96-103.

11. Faber J, Schaprian T, Berkan K, et al. Regional brain and spinal cord volume loss in spinocerebellar ataxia type 3. Mov Disord. 2021;36:2273-2281.

12. Wu X, Liao X, Zhan Y, et al. Microstructural alterations in asymptomatic and symptomatic patients with spinocerebellar ataxia type 3: a tract-based spatial statistics study. Front Neurol. 2017;8:714.

13. Rezende TJR, de Paiva JLR, Martinez ARM, et al. Structural signature of SCA3: from presymptomatic to late disease stages. Ann Neurol. 2018;84(3):401-408.

14. Joers JM, Deelchand DK, Lyu T, et al. Neurochemical abnormalities in premanifest and early spinocerebellar ataxias. Ann Neurol. 2018;83(4):816-829.

15. Rubinov M, Sporns O. Complex network measures of brain connectivity: uses and interpretations. Neuroimage. 2010;52(3):1059-1069.

16. Wu YT, Huang SR, Jao CW, et al. Impaired efficiency and resilience of structural network in spinocerebellar ataxia type 3. Front Neurosci. 2018;12:935.

17. Shah A, Prasad S, Rastogi B, et al. Altered structural connectivity of the motor subnetwork in multiple system atrophy with cerebellar features. Eur Radiol. 2019;29 (6):2783-2791.

18. Pardini M, Yaldizli O, Sethi V, et al. Motor network efficiency and disability in multiple sclerosis. Neurology. 2015;85(13):1115-1122.

19. Tournier JD, Calamante F, Connelly A. MRtrix: diffusion tractography in crossing fiber regions. Int J Imaging Syst Technol. 2012;22(1):53-66.

20. Salmon E, Van der Linden MV, Franck G. Anterior cingulate and motor network metabolic impairment in progressive supranuclear palsy. Neuroimage. 1997;5 (3):173-178.

21. Xiao R, Malekmohammadi M, Pouratian N, Hu X. Characterization of pallidocortical motor network in Parkinson's disease through complex network analysis. J Neural Eng. 2019;16(6):066034.

22. Novaes NP, Balardin JB, Hirata FC, et al. Global efficiency of the motor network is decreased in Parkinson's disease in comparison with essential tremor and healthy controls. Brain Behav. 2021;11(8):e02178.

23. Leodori G, De Bartolo MI, Guerra A, et al. Motor cortical network excitability in Parkinson's disease. Mov Disord. 2022;37(4):734-744.

24. Olivito G, Cercignani M, Lupo M, et al. Neural substrates of motor and cognitive dysfunctions in SCA2 patients: a network based statistics analysis. NeuroimageClin. 2017;14:719-725.

25. Zalesky A, Fornito A, Bullmore ET. Network-based statistic: identifying differences in brain networks. Neuroimage. 2010;53(4):1197-1207.

26. Woolrich MW, Jbabdi S, Patenaude B, et al. Bayesian analysis of neuroimaging data in FSL. Neuroimage. 2009;45(1 Suppl):S173-S186.

27. Desikan RS, Segonne F, Fischl B, et al. An automated labeling system for subdividing the human cerebral cortex on MRI scans into gyral based regions of interest. Neuroimage. 2006;31(3):968-980.

28. Dale AM, Fischl B, Sereno MI. Cortical surface-based analysis: I. segmentation and surface reconstruction. Neuroimage. 1999;9(2):179-194.

29. Diedrichsen J. A spatially unbiased atlas template of the human cerebellum. Neuroimage. 2006;33(1):127-138.

30. Diedrichsen J, Balsters JH, Flavell J, Cussans E, Ramnani N. A probabilistic MR atlas of the human cerebellum. Neuroimage. 2009;46(1):39-46.

31. Tournier JD, Smith R, Raffelt D, et al. MRtrix3: a fast, flexible and open software framework for medical image processing and visualisation. Neuroimage. 2019;202:116137.

32. Andersson JLR, Sotiropoulos SN. An integrated approach to correction for off-resonance effects and subject movement in diffusion MR imaging. Neuroimage. 2016 Jan;15(125):1063-1078.

33. Andersson JLR, Graham MS, Zsoldos E, Sotiropoulos SN. Incorporating outlier detection and replacement into a non-parametric framework for movement and distortion correction of diffusion MR images. Neuroimage. 2016;141:556-572.

34. Andersson JLR, Graham MS, Drobnjak I, Zhang H, Filippini N, Bastiani M. Towards a comprehensive framework for movement and distortion correction of diffusion MR images: within volume movement. Neuroimage. 2017;152:450-466.

35. Tustison NJ, Avants BB, Cook PA, et al. N4ITK: improved N3 bias correction. IEEE Trans Med Imaging. 2010;29 (6):1310-1320.

36. Kamagata K, Zalesky A, Hatano T, et al. Connectome analysis with diffusion MRI in idiopathic Parkinson's disease: evaluation using multi-shell, multi-tissue, constrained spherical deconvolution. NeuroimageClin. 2018;17:518-529.

37. Tournier J-D, Calamante F, Connelly A. Improved probabilistic streamlines tractography by 2nd order integration over fibre orientation distributions. Proceedings of the International Society for Magnetic Resonance in Medicine. Vol 1670. John Wiley & Sons, Inc; 2010.

38. Smith RE, Tournier JD, Calamante F, Connelly A. Anatomically-constrained tractography: improved diffusion MRI streamlines tractography through effective use of anatomical information. Neuroimage. 2012;62 (3):1924-1938.

39. Smith RE, Tournier J-D, Calamante F, Connelly A. SIFT2: enabling dense quantitative assessment of brain white matter connectivity using streamlines tractography. Neuroimage. 2015;119:338-351.

40. Watson CG, DeMaster D, Ewing-Cobbs L. Graph theory analysis of DTI tractography in children with traumatic injury. NeuroimageClin. 2019;21:101673.

41. Newman ME. The structure and function of complex networks. SIAM Rev. 2003;45(2):167-256.

42. Ingalhalikar M, Smith A, Parker D, et al. Sex differences in the structural connectome of the human brain. Proc Natl Acad Sci U S A. 2014;111(2):823-828.

43. Li X, Steffens DC, Potter GG, Guo H, Song S, Wang L. Decreased between-hemisphere connectivity strength and network efficiency in geriatric depression. Hum Brain Mapp. 2017;38(1):53-67.

44. Frossard J, Renaud O. Permuco: permutation tests for regression, (repeated measures) ANOVA/ANCOVA and comparison of signals. 2019.

45. Kohl M. MKinfer: Inferential Statistics (R Package version 0.6). 2020. http://www.stamats.de/

46. Newman ME. Assortative mixing in networks. Phys Rev Lett. 2002;89(20):208701.

47. Craig BT, Hilderley A, Kinney-Lang E, Long X, Carlson HL, Kirton A. Developmental neuroplasticity of the white matter connectome in children with perinatal stroke. Neurology. 2020;95(18):e2476-e2486.

48. Zalesky A, Akhlaghi H, Corben LA, et al. Cerebello-cerebral connectivity deficits in Friedreich ataxia. Brain Struct Funct. 2014;219(3):969-981.

49. Hernandez-Castillo CR, Galvez V, Mercadillo RE, et al. Functional connectivity changes related to cognitive and motor performance in spinocerebellar ataxia type 2. Mov Disord. 2015;30(10):1391-1399.

50. Li M, Chen X, Xu HL, et al. Brain structural abnormalities in the preclinical stage of Machado-Joseph disease/ spinocerebellar ataxia type 3 (MJD/SCA3): evaluation by MRI morphometry, diffusion tensor imaging and neurite orientation dispersion and density imaging. J Neurol. 2022;269(6):2989-2998.

51. Yen T-C, Tzen K-Y, Chen M-C, et al. Dopamine transporter concentration is reduced in asymptomatic Machado-Joseph disease gene carriers. J Nucl Med. 2002;43(2):153-159.

52. Lee H, Kim HA. Nystagmus in SCA territory cerebellar infarction: pattern and a possible mechanism. J Neurol Neurosurg Psychiatry. 2013;84(4):446-451.

53. Raposo M, Vasconcelos J, Bettencourt C, Kay T, Coutinho P, Lima M. Nystagmus as an early ocular alteration in Machado-Joseph disease (MJD/SCA3). BMC Neurol. 2014;14:17.

54. Piccinin CC, Rezende TJR, de Paiva JLR, et al. A 5-year longitudinal clinical and magnetic resonance imaging study in spinocerebellar ataxia type 3. Mov Disord. 2020;35(9):1679-1684.

55. Bostan AC, Strick PL. The basal ganglia and the cerebellum: nodes in an integrated network. Nat Rev Neurosci. 2018;19(6):338-350.

56. Guo J, Chen H, Biswal BB, et al. Gray matter atrophy patterns within the cerebellum-neostriatum-cortical network in SCA3. Neurology. 2020;95(22):e3036-e3044.

57. Fasano A, Herzog J, Raethjen J, et al. Gait ataxia in essential tremor is differentially modulated by thalamic stimulation. Brain. 2010;133(Pt 12):3635-3648.

58. Reich MM, Brumberg J, Pozzi NG, et al. Progressive gait ataxia following deep brain stimulation for essential tremor: adverse effect or lack of efficacy? Brain. 2016;139 (11):2948-2956.

59. Choe CU, Hidding U, Schaper M, et al. Thalamic short pulse stimulation diminishes adverse effects in essential tremor patients. Neurology. 2018;91(8):e704-e713.

60. Jones DK. Diffusion MRI: Theory, Methods, and Applications. Oxford University Press; 2011.

61. Jones R, Grisot G, Augustinack J, et al. Insight into the fundamental trade-offs of diffusion MRI from polarization-sensitive optical coherence tomography in ex vivo human brain. Neuroimage. 2020;214:116704.

62. Carass A, Cuzzocreo JL, Han S, et al. Comparing fully automated state-of-the-art cerebellum parcellation from magnetic resonance images. Neuroimage. 2018;183:150-172.